Fast Steady-State Analysis for Droop-Controlled AC Microgrid

Jun Zhang
Electrical Engineering and Computer Science
South Dakota State University
Brookings, USA
Jun.Zhang@jacks.sdstate.edu

Junjian Qi
Electrical Engineering and Computer Science
South Dakota State University
Brookings, USA
Junjian.Qi@sdstate.edu

***Abstract*—Simplicity and communication independence make droop control a prevalent choice in industry. Understanding its steady state gains importance with the increasing size of microgrids. This paper proposes a fast approach for calculating the steady state of the droop-controlled AC microgrid. First, linear power flow equations are used to simplify the problem. Second, the closed-form steady-state solution is derived given a specific system frequency. Third, to fully consider the load and network loss changes due to frequency deviations, an algorithm is developed for fast assessing of the steady state by frequency updating based on droop equations in each iteration. Simulation results on two test systems demonstrate that the proposed method can provide a rapid solution with acceptable accuracy.**

***Index Terms*—AC microgrid, droop control, frequency deviation, power flow equation, steady-state analysis.**

I. Introduction

Microgrids integrate multiple distributed generators (DGs), battery storage systems, and loads, operating in either grid-connected or islanded mode [1]. As the focus on utilizing renewable energy continues to grow, microgrids are emerging as a vital platform for renewable energy consumption. Droop control is the most traditional control strategy deployed for microgrids. It is proposed as a primary control to achieve power sharing among DGs by emulating the inertial behavior of synchronous generators. Although droop control is operationally simple, it suffers from load-dependent frequency and voltage deviations, inappropriate reactive power sharing, and poor dynamic performance [2], [3].

To address these problems, many control strategies emerge. Virtual impedance based method [4] is designed to compensate for the feeder impedance difference and reduce the reactive power sharing mismatch. To achieve proportional active and reactive power sharing, droop-based secondary controls are proposed in [5]–[7]. Recently, droop-free controls have also been proposed in which the primary-level droop control is eliminated [2], [3], [8].

Despite the emergence of these advanced controls, the conventional droop control is still the most well-tested and applied control in reality. Due to its simplicity and ability to operate independently of communication, it serves as the primary control layer in the control hierarchy, ensuring rapid response and frequency/voltage stability.

With the fast expanding of microgrids, the steady-state analysis for droop-controlled microgrid system becomes critical, which provides information of the overall system by solving power flow equations. On one hand, an accurate steady-state analysis is required for control performance evaluation, parameters tuning, small-signal analysis initialization, and microgrid planning. On the other hand, a fast, simplified method is necessary for real-time dispatch and contingency analysis.

Conventional power flow equations cannot be directly applied to analyze the steady state of the droop-controlled AC microgrid. In conventional power flow, buses are classified into slack, PV, and PQ buses, ensuring the number of variables is equal to the number of equations. However, this classification is not valid for the droop-controlled microgrid: 1) The terminal voltage of the inverter bus is not constant; 2) The system frequency may not be nominal; 3) The inverters' output active and reactive powers are not constant.

Several methods have been proposed for the steady-state analysis of the droop-controlled microgrid. In [9], the phase angle droop and voltage droop are considered in the power flow equations. However, phase angle droop is not usually used. In [10], the steady state is calculated by iterations including *dq* frame calculation for inverter output and *xy* frame for network impedance, voltage, and current. However, this method requires heavy computation. In [11], a slack bus is assumed in the microgrid and two nested loops are involved in the iteration to repeatedly solve the power flow equations to eliminate the unbalance of active power and voltage in the assumed slack bus until accuracy is acceptable. However, the massive power flow calculation largely increases the computation burden. In [12], a current injection method is used to model the load and network changes. But this method is still complicated and is not compatible with the typical power flow equations.

In [13], the droop control with virtual impedance is considered and frequency is considered as a global variable. Loads are modeled as functions of frequency to guarantee accuracy. However, the network loss change is ignored and the feeder parameters are treated as constants. In the distribution system, with a large R/X ratio, ignoring the network loss change will

This work was supported by the National Science Foundation under ECCS-2403660.

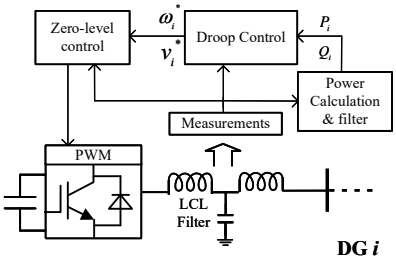

Fig. 1. Typical structure of grid-forming inverter with droop control.

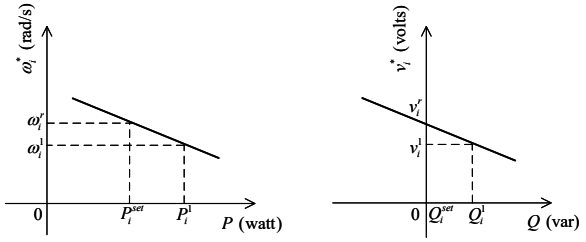

(a) P-f loop (b) Q-V loop

Fig. 2. Droop characteristics.

inevitably impact the steady state accuracy.

With the methods mentioned above, a fast and simplified steady-state analysis for droop-controlled AC microgrid is lacking. To this end, in this paper we propose a method for fast-steady state analysis of the droop-controlled AC microgrid with high efficiency and acceptable accuracy, considering network and load parameter change under different frequencies. The main contributions are summarized as follows.

1) Linear power flow equations are used to simplify the calculation. A closed-form solution for droop-controlled AC microgrid under a specific system frequency is derived to speed up the solving process.
2) A fast algorithm is developed to calculate the final frequency. The changes in load and network parameters caused by frequency deviation are considered to improve the steady-state analysis accuracy.

The remainder of this paper is organized as follows. Section II introduces the conventional droop control mechanism. Section III describes the typical accurate method to calculate the steady state of the droop-controlled AC microgrid. Section IV introduces our proposed fast steady-state analysis method. Section V presents the simulation results. Finally, conclusions are drawn in Section VI.

II. Conventional Droop Control

A. Inverter Control Structure

Grid-forming inverter operates as a voltage source that controls its voltage and frequency to support the microgrid. The typical grid-forming inverter with droop control is shown in Fig. 1. DG i calculates its active power output P_i and reactive power output Q_i by the power calculation block. Depending on the filtered P_i and Q_i, droop control decides the final set points v_i^* and ω_i^*, and then feeds them into the zero-level control (e.g., double-loop control). Then the modulation wave is generated to produce the pulse width modulation (PWM) signal to drive the inverter.

B. Conventional Grid-Forming Droop Control

The typical power-frequency *(P-f)* droop and var-voltage *(Q-V)* droop for deciding the final set points are illustrated in Fig. 2 [14]. They regulate the frequency and terminal voltage of the inverter as:

$$\omega_i^* = \omega_i^{\mathrm{r}} - m_{p_i}\left(P_i - P_i^{\mathrm{set}}\right) \tag{1}$$

$$v_i^* = v_i^{\mathrm{r}} - m_{q_i}(Q_i - Q_i^{\mathrm{set}}), \tag{2}$$

where ω_i^{r} and v_i^{r} are the frequency and voltage references; m_{p_i} and m_{q_i} are the frequency and voltage droop coefficients; and P_i^{set} and Q_i^{set} are the active and reactive power set points. Based on the current active and reactive power outputs, droop control mimics the generator's behavior by changing the DG's frequency and voltage. For example, as shown in Fig. 2, when $P_i > P_i^{\mathrm{set}}$, droop control lowers the frequency set point ω_i^*. Similarly, when $Q_i > Q_i^{\mathrm{set}}$, droop control lowers the voltage set point v_i^*. Here P_i^{set} and Q_i^{set} are local constant data that are selected as an ideal operating point. It is clear that the frequency and voltage may not be equal to the pre-assigned reference values, resulting in frequency and voltage deviations.

III. Accurate Steady-State Calculation for Droop-Controlled AC Microgrid

Here we show the method to calculate the accurate steady state for an AC microgrid with droop control. As the system frequency will not necessarily be the nominal frequency under droop control, the feeder and load impedances are not constant but functions of ω^*, meaning that the admittance matrix is also a function of ω^*. Let the buses be those in the middle of the LCL filter of each source and the other buses are eliminated by Kron reduction. Let the set of the remaining buses be $\mathcal{N} = \{1, \cdots, N\}$ where N is the number of DGs. Then the bus admittance matrix for the reduced network is denoted by $\mathbf{Y}(\omega^*) = \mathbf{G}(\omega^*) + \mathrm{j}\mathbf{B}(\omega^*)$.

Let $G_{ij}(\omega^*)$ and $B_{ij}(\omega^*)$ be the real and imaginary parts of $Y_{ij}(\omega^*)$, respectively. Then the AC power flow equations under ω^* for $\forall i \in \mathcal{N}$ can be described as:

$$P_i = v_i^* \sum_{j=1}^{N} v_j^* \Big(G_{ij}(\omega^*)\cos\delta_{ij} + B_{ij}(\omega^*)\sin\delta_{ij} \Big) \tag{3}$$

$$Q_i = v_i^* \sum_{j=1}^{N} v_j^* \Big(G_{ij}(\omega^*)\sin\delta_{ij} - B_{ij}(\omega^*)\cos\delta_{ij} \Big), \tag{4}$$

where P_i and Q_i are the active and reactive powers of the ith DG, v_i^* and v_j^* are, respectively, the voltage magnitudes of buses i and j, $\delta_{ij} = \delta_i - \delta_j$ is the phase angle difference between buses i and j.

Unlike the bus types in conventional power flow analysis in which the buses provide either constant v_i^* and P_i or constant P_i and Q_i to make sure that the number of variables and

the number of equations are equal, the DG buses with droop control provide additional 'constraints' on the final steady state. At the steady state, the two droop control equations (1)–(2) must be satisfied. Since the system should operate synchronously, all DGs must share the same global frequency ω^* at the steady state. Therefore, the droop control adds $2N$ additional equations in (5a)–(5b) to the power flow equations in (3)–(4) to ensure a final steady state as [13], [15]:

$$\begin{cases} \omega^* = \omega_i^{\mathrm{r}} - m_{p_i}\left(P_i - P_i^{\mathrm{set}}\right) = \omega_j^{\mathrm{r}} - m_{p_j}\left(P_j - P_j^{\mathrm{set}}\right) & \text{(5a)} \\ \qquad\qquad i,j \in \mathcal{N}, i \neq j & \\ v_i^* = v_i^{\mathrm{r}} - m_{q_i}\left(Q_i - Q_i^{\mathrm{set}}\right), i \in \mathcal{N} & \text{(5b)} \\ \text{(3)–(4).} & \text{(5c)} \end{cases}$$

Setting δ_1 as the reference angle, there are a total of $4N$ equations with $4N$ variables, $\omega^*, v_1^*, \cdots, v_N^*$, $\delta_2, \cdots, \delta_N, P_1, \cdots, P_N, Q_1, \cdots, Q_N$, to be solved for.

IV. Fast Steady-State Calculation

A. Linear Power Flow Equations

Due to the nonlinearity, directly solving (5) is challenging and time-consuming for a large microgrid. Therefore, a linear equation system is more desirable for a simple and fast calculation. In (5), the nonlinearity comes from the AC power flow equations. The linear power flow model in [16] has been shown to be accurate and robust for distribution systems. We use this model to simplify (3)–(4) as:

$$P_i = \sum_{j=1}^{N}\Big(G_{ij}(\omega^*)v_j^* - B_{ij}(\omega^*)\delta_j\Big) \tag{6}$$

$$Q_i = -\sum_{j=1}^{N}\Big(B_{ij}(\omega^*)v_j^* + G_{ij}(\omega^*)\delta_j\Big), \tag{7}$$

where the global frequency ω^* is still involved. Using (6)–(7) can largely simplify the power flow equations and speed up the calculation. However, due to the existence of the global frequency ω^*, (6) and (7) will still be nonlinear.

B. Approximate Linear Equations

To further simplify the problem, we first use constant $\mathbf{G}$ and $\mathbf{B}$ at the nominal frequency, ω_0, assuming that the frequency deviation is small. Then we have the following linear equation system that defines the final steady state:

$$\begin{cases} \omega_i^{\mathrm{r}} - m_{p_i}\left(P_i - P_i^{\mathrm{set}}\right) & \text{(8a)} \\ \qquad = \omega_j^{\mathrm{r}} - m_{p_j}\left(P_j - P_j^{\mathrm{set}}\right), i,j \in \mathcal{N}, i \neq j & \\ v_i^* = v_i^{\mathrm{r}} - m_{q_i}\left(Q_i - Q_i^{\mathrm{set}}\right), i \in \mathcal{N} & \text{(8b)} \\ P_i = \sum_{j=1}^{N}\Big(G_{ij}(\omega_0)v_j^* - B_{ij}(\omega_0)\delta_j\Big), i \in \mathcal{N} & \text{(8c)} \\ Q_i = -\sum_{j=1}^{N}\Big(B_{ij}(\omega_0)v_j^* + G_{ij}(\omega_0)\delta_j\Big), i \in \mathcal{N}. & \text{(8d)} \end{cases}$$

Define the vector of the variables to be solved for as:

$$\mathbf{x} = [\mathbf{v}^\top\ \boldsymbol{\delta}^\top\ \mathbf{P}^\top\ \mathbf{Q}^\top]^\top, \tag{9}$$

where

$$\mathbf{v} = [v_1^*, v_2^*, \cdots, v_N^*]^\top \tag{10}$$

$$\boldsymbol{\delta} = [\delta_1, \delta_2, \cdots, \delta_N]^\top \tag{11}$$

$$\mathbf{P} = [P_1, P_2, \cdots, P_N]^\top \tag{12}$$

$$\mathbf{Q} = [Q_1, Q_2, \cdots, Q_N]^\top. \tag{13}$$

Then (8a)–(8b) can be written as:

$$\mathbf{A}_{\omega p}\mathbf{P} = \mathbf{b}_\omega \tag{14}$$

$$\mathbf{v} + \mathbf{A}_{v^* q}\mathbf{Q} = \mathbf{b}_v, \tag{15}$$

where

$$\mathbf{A}_{\omega p} = \begin{bmatrix} -m_{p_1} & m_{p_2} & \cdots & & 0 \\ \vdots & -m_{p_2} & m_{p_3} & & \vdots \\ & & \ddots & \ddots & \\ 0 & \cdots & & -m_{p_{(N-1)}} & m_{p_N} \end{bmatrix} \tag{16}$$

$$\mathbf{b}_\omega = \begin{bmatrix} \omega_2^{\mathrm{r}} - \omega_1^{\mathrm{r}} + m_{p_2}P_2^{\mathrm{set}} - m_{p_1}P_1^{\mathrm{set}} \\ \omega_3^{\mathrm{r}} - \omega_2^{\mathrm{r}} + m_{p_3}P_3^{\mathrm{set}} - m_{p_2}P_2^{\mathrm{set}} \\ \vdots \\ \omega_N^{\mathrm{r}} - \omega_{N-1}^{\mathrm{r}} + m_{p_N}P_N^{\mathrm{set}} - m_{p_{(N-1)}}P_{N-1}^{\mathrm{set}} \end{bmatrix} \tag{17}$$

$$\mathbf{A}_{v^* q} = \mathrm{diag}\big([m_{q_1}, m_{q_2}, \cdots, m_{q_N}]\big) \tag{18}$$

$$\mathbf{b}_{v^*} = \begin{bmatrix} v_1^{\mathrm{r}} + m_{q_1}Q_1^{\mathrm{set}} \\ v_2^{\mathrm{r}} + m_{q_2}Q_2^{\mathrm{set}} \\ \vdots \\ v_N^{\mathrm{r}} + m_{q_N}Q_N^{\mathrm{set}} \end{bmatrix}. \tag{19}$$

Further, (8c)–(8d) can be written in compact form as:

$$\mathbf{P} = \mathbf{G}(\omega_0)\,\mathbf{v} - \mathbf{B}(\omega_0)\,\boldsymbol{\delta} \tag{20}$$

$$\mathbf{Q} = -\mathbf{B}(\omega_0)\,\mathbf{v} - \mathbf{G}(\omega_0)\,\boldsymbol{\delta}. \tag{21}$$

In addition, we add the following equation to set the first phase angle as 0:

$$\mathbf{A}_{\delta_0\delta}\boldsymbol{\delta} = 0, \tag{22}$$

where

$$\mathbf{A}_{\delta_0\delta} = [1\ \ \mathbf{0}_{1\times(N-1)}]. \tag{23}$$

Then the compact form of the linear equations in (8) is:

$$\mathbf{A}\mathbf{x} = \mathbf{b}, \tag{24}$$

where

$$\mathbf{A} = \begin{bmatrix} \mathbf{0} & \mathbf{A}_{\delta_0\delta} & \mathbf{0} & \mathbf{0} \\ \mathbf{0} & \mathbf{0} & \mathbf{A}_{\omega p} & \mathbf{0} \\ \mathbf{I}_{N\times N} & \mathbf{0} & \mathbf{0} & \mathbf{A}_{v^* q} \\ \mathbf{G}(\boldsymbol{\omega_0}) & -\mathbf{B}(\boldsymbol{\omega_0}) & -\mathbf{I}_{N\times N} & \mathbf{0} \\ -\mathbf{B}(\boldsymbol{\omega_0}) & -\mathbf{G}(\boldsymbol{\omega_0}) & \mathbf{0} & -\mathbf{I}_{N\times N} \end{bmatrix} \tag{25}$$

$$\mathbf{b} = \begin{bmatrix} 0 & \mathbf{b}_\omega^\top & \mathbf{b}_{v^*}^\top & \mathbf{0}_N^\top & \mathbf{0}_N^\top \end{bmatrix}^\top, \tag{26}$$

and $\mathbf{I}_{N\times N}$ is an identity matrix.

Since there are $4N$ equations and $4N$ variables in (24), it will produce a closed-form unique solution if there is any. The

accuracy of the solution is acceptable if each DG is outputting the same active power output as its set point; otherwise, iterations as presented in the next subsection are needed.

C. Frequency Update and Overall Algorithm

The solution of (24) does not consider the change of the load and network parameters under different system frequencies. To address this problem and improve the accuracy, we update the system frequency when the first equation in (5a) is not satisfied. With nominal frequency ω_0, solving (24) can estimate the active power of each DG. Then the approximated frequency $\omega^{*(1)}$ can be calculated by (5a). By setting the frequency as the new system frequency $\omega^{*(1)}$, we can resolve (24) to get a better solution. This process can be described by Algorithm 1 as shown below until the required accuracy

$$\Delta\omega^{*(k)} = \left|\omega^{*(k)} - \omega^{*(k-1)}\right| \tag{27}$$

is less than a predetermined threshold ϵ, where k denotes the current iteration and $\omega^{*(k)}$ is the ω^* value in iteration k.

Algorithm 1: Fast steady-state calculation for droop-controlled AC microgrid

Initialization: Set $k = 0$, $\omega^{*(0)} = \omega_0$
while $k < k_{\max}$ **do**
  Calculate $\mathbf{G}\left(\omega^{*(k)}\right)$ and $\mathbf{B}\left(\omega^{*(k)}\right)$
  Solve (24)
  Set $k = k + 1$
  Update $\omega^{*(k)}$ based on (5a)
  Calculate $\Delta\omega^{*(k)}$ based on (27)
  if $\Delta\omega^{*(k)} < \epsilon$ **then**
    break
  end
end

Remark. *Although the fast method may require iteration, the final system frequency can be reached by only several iterations though* (5a)*. Since* (24) *is linear, this method will be fast compared with the accurate method especially when the system size is large. The only error will be produced by the power flow approximation in* (6) *and* (7) *which has been proved acceptable in [16] for distribution systems.*

V. Simulation Results

A. Test on A 4-DG Microgrid System

A modified 4-DG test system is shown in Fig. 3. The grid parameters are the same as those in [3] except that the line resistances are four times of the original values (R/X ranges from 2.6 to 4.9) to simulate the highly resistive low-voltage distribution system with $R \gg X$. The system and droop control parameters are listed in Table I.

Simulation is performed in Matlab/Simulink at a time-step of 50 μs using the fixed-step discrete ODE-4 solver. The inverter model is selected as the average model to eliminate the harmonics in the simulation.

To validate the proposed method, the results calculated by the accurate method in Section III and the proposed fast method in Section IV are compared with the result from Simulink simulation. Both normal and heavy loading conditions are considered to show the robustness of the proposed method under different frequency deviations. As shown in

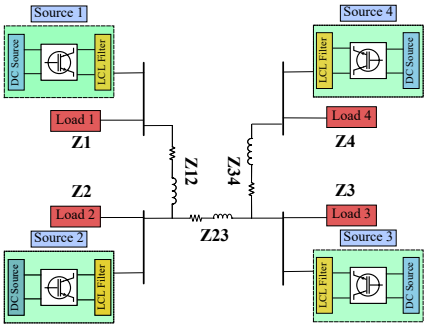

Fig. 3. Modified 4-DG test system.

TABLE I
4-DG System and Droop Control Parameters

Symbol	Description	Value
Z_{12}	Line 1–2 resistance and inductance	3.2 Ω, 0.0036 H
Z_{23}	Line 2–3 resistance and inductance	1.6 Ω, 0.0018 H
Z_{34}	Line 3–4 resistance and inductance	2.8 Ω, 0.0015 H
Z_1	Load 1 resistance and inductance (normal/heavy)	32.8823Ω, 0.0308H / 9.986 Ω, 0.0007H
Z_2	Load 2 resistance and inductance (normal/heavy)	42.747Ω, 0.0401H / 11.9832 Ω, 0.0008H
Z_3	Load 3 resistance and inductance (normal/heavy)	45.5683Ω, 0.0133H / 11.9958 Ω, 0.0004H
Z_4	Load 4 resistance and inductance (normal/heavy)	50.6315Ω, 0.0148H / 9.9965 Ω, 0.0004H
m_{p_i}	Frequency droop	0.0009 rad/(W·s)
m_{q_i}	Voltage droop	0.004 Var/V
ω_i^{r}	Frequency references	120π (rad/s)
v_i^{r}	Voltage references	120 V
P_i^{set}	Active power set points	1000 W
Q_i^{set}	Reactive power set points	0 Var

TABLE II
The Solution under Normal Load

Simulink		Accurate Method		Fast Method	
v (p.u.)	**δ (rad)**	**v (p.u.)**	**δ (rad)**	**v (p.u.)**	**δ (rad)**
0.9878	0	0.9878	0	0.9877	0
0.9939	0.0141	0.9939	0.0141	0.9941	0.0141
0.9962	0.0176	0.9962	0.0176	0.9965	0.0177
0.9994	0.0245	0.9994	0.0245	1.0000	0.025
f (Hz)	60.0084		60.0084		60.0073

TABLE III
The Solution under Heavy Load

Simulink		Accurate Method		Fast Method	
v (p.u.)	**δ (rad)**	**v (p.u.)**	**δ (rad)**	**v (p.u.)**	**δ (rad)**
0.9877	0	0.9877	0	0.9878	0
0.9972	0.0218	0.9972	0.0218	0.9989	0.022
0.9975	0.0202	0.9975	0.0202	0.9992	0.0206
0.988	0.0026	0.988	0.0026	0.9883	0.0027
f (Hz)	59.5928		59.5928		59.588

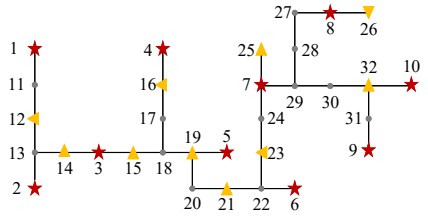

Fig. 4. Modified IEEE 34-bus test system (stars indicate DGs and triangles indicate loads).

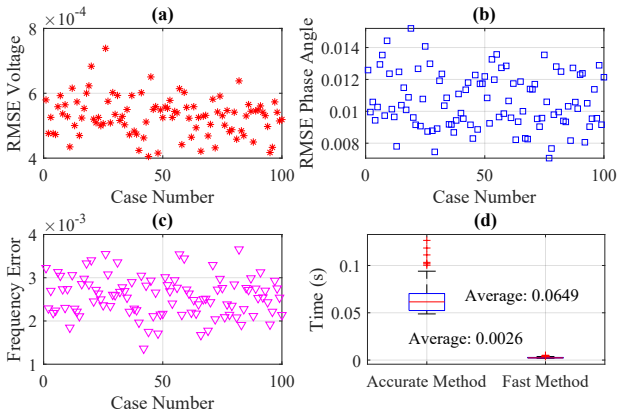

Fig. 5. Comparison between the proposed fast method and accurate method: (a) voltage RMSE; (b) phase angle RMSE; (c) frequency error; (d) runtime.

Tables II–III, the accurate method can get the same steady state as the Simulink simulation. The proposed fast steady-state analysis method can get a steady state that is very close to that from the Simulink simulation.

B. Test on the Modified IEEE 34-Bus System

We test our proposed method on the modified IEEE 34-bus test system [8], as shown in Fig. 4. The tests are performed in Matlab 2020b on a laptop computer with Intel Core i7-1065G7 CPU @1.3GHz and 8GB RAM. The accurate method is implemented using the trust region method, initiated from a flat start and with an accuracy tolerance of 10^{-6}. For the proposed fast method, $\epsilon = 10^{-6}$. The droop control parameters are the same as those in Table I. Both methods are run for 100 cases for each of which a random load change following a normal distribution with zero mean and 10% standard deviation is added to the initial loads' resistance and inductance.

The voltage and phase angle root mean square error (RMSE) of the proposed fast method compared with the accurate method under the 100 cases are shown in Figs. 5 (a)–(b). The voltage of the proposed method is almost the same as the accurate method. The phase angle RMSE is also acceptable. As in Fig. 5 (c), the steady-state frequency error, defined as the absolute difference between these two methods, is small.

As shown in Fig. 5(d), the proposed fast method only takes 0.0026 s on average while the accurate method needs 0.0649 s, achieving a speed-up of almost 25. This clearly demonstrates the advantage of the proposed fast method in efficient steady-state analysis of the droop-controlled AC microgrid.

VI. Conclusion

This paper proposes a fast method to calculate the steady state of the droop-controlled AC microgrid. To speed up the calculation and consider the network changes due to frequency deviation, linear power flow equations are involved, a closed-form formula is derived for a given frequency, and an algorithm is developed for frequency updating. The simulations on a 4-DG microgrid system and the modified IEEE 34-bus system show that the proposed method can obtain accurate enough steady states with greatly improved time efficiency, achieving a speed-up of almost 25 for the IEEE 34-bus system.

References

[1] Z. Wang, W. Wu, and B. Zhang, "A distributed quasi-newton method for droop-free primary frequency control in autonomous microgrids," *IEEE Trans. Smart Grid*, vol. 9, no. 3, pp. 2214–2223, May 2018.

[2] V. Nasirian, Q. Shafiee, J. M. Guerrero, F. L. Lewis, and A. Davoudi, "Droop-free distributed control for AC microgrids," *IEEE Trans. Power Electron.*, vol. 31, no. 2, pp. 1600–1617, Feb. 2016.

[3] S. M. Mohiuddin and J. Qi, "Droop-free distributed control for AC microgrids with precisely regulated voltage variance and admissible voltage profile guarantees," *IEEE Trans. Smart Grid*, vol. 11, no. 3, pp. 1956–1967, May 2020.

[4] W. Deng, N. Dai, K.-W. Lao, and J. M. Guerrero, "A virtual-impedance droop control for accurate active power control and reactive power sharing using capacitive-coupling inverters," *IEEE Trans. Ind. Appl.*, vol. 56, no. 6, pp. 6722–6733, July 2020.

[5] A. D. Dominguez-Garcia, C. N. Hadjicostis, and N. H. Vaidya, "Resilient networked control of distributed energy resources," *IEEE J. Sel. Areas Commun.*, vol. 30, no. 6, pp. 1137–1148, July 2012.

[6] B. A. Robbins, C. N. Hadjicostis, and A. D. Dominguez-Garcia, "A two-stage distributed architecture for voltage control in power distribution systems," *IEEE Trans. Power Syst.*, vol. 28, no. 2, pp. 1470–1482, May 2013.

[7] A. Bidram, A. Davoudi, and F. L. Lewis, "A multiobjective distributed control framework for islanded AC microgrids," *IEEE Trans. Ind. Inform.*, vol. 10, no. 3, pp. 1785–1798, Aug. 2014.

[8] S. M. Mohiuddin and J. Qi, "Optimal distributed control of AC microgrids with coordinated voltage regulation and reactive power sharing," *IEEE Trans. Smart Grid*, vol. 13, no. 3, pp. 1789–1800, May 2022.

[9] C. Wang, B. Cui, and Z. Wang, "Analysis of solvability boundary for droop-controlled microgrids," *IEEE Trans. Power Syst.*, vol. 33, no. 5, pp. 5799–5802, Sept. 2018.

[10] J. A. Mueller and J. W. Kimball, "An efficient method of determining operating points of droop-controlled microgrids," *IEEE Trans. Energy Convers.*, vol. 32, no. 4, pp. 1432–1446, Dec. 2017.

[11] G. C. Kryonidis, E. O. Kontis, A. I. Chrysochos, K. O. Oureilidis, C. S. Demoulias, and G. K. Papagiannis, "Power flow of islanded AC microgrids: Revisited," *IEEE Trans. Smart Grid*, vol. 9, no. 4, pp. 3903–3905, July 2018.

[12] O. Bassey, C. Chen, and K. L. Butler-Purry, "Linear power flow formulations and optimal operation of three-phase autonomous droop-controlled microgrids," *Electr. Power Syst. Res.*, vol. 196, July 2021.

[13] C. Li, S. K. Chaudhary, M. Savaghebi, J. C. Vasquez, and J. M. Guerrero, "Power flow analysis for low-voltage AC and DC microgrids considering droop control and virtual impedance," *IEEE Trans. Smart Grid*, vol. 8, no. 6, pp. 2754–2764, Nov. 2017.

[14] J. M. Guerrero, J. C. Vasquez, J. Matas, L. G. de Vicuna, and M. Castilla, "Hierarchical control of droop-controlled AC and DC microgrids—a general approach toward standardization," *IEEE Trans. Ind. Electron.*, vol. 58, no. 1, pp. 158–172, Jan. 2011.

[15] M. M. A. Abdelaziz, H. E. Farag, E. F. El-Saadany, and Y. A.-R. I. Mohamed, "A novel and generalized three-phase power flow algorithm for islanded microgrids using a newton trust region method," *IEEE Trans. Power Syst.*, vol. 28, no. 1, pp. 190–201, Feb. 2013.

[16] J. Yang, N. Zhang, C. Kang, and Q. Xia, "A state-independent linear power flow model with accurate estimation of voltage magnitude," *IEEE Trans. Power Syst.*, vol. 32, no. 5, pp. 3607–3617, Sept. 2017.